Chin. J. Astron. Astrophys. Vol. 6 (2006), No. 6, 669–679
(*http://www.chjaa.org*)

Chinese Journal of
Astronomy and
Astrophysics

A Study of Binary Stellar Population Synthesis of Elliptical Galaxies *

Zhong-Mu Li[1,2], Feng-Hui Zhang[1] and Zhan-Wen Han[1]

[1] National Astronomical Observatories / Yunnan Observatory, Chinese Academy of Sciences, Kunming 650011; *zhongmu.li@gmail.com*
[2] Graduate School of Chinese Academy of Sciences, Beijing 100049

Received 2006 February 17; accepted 2006 April 12

Abstract We determined the relative stellar ages and metallicities of about 80 elliptical galaxies in both low and high density environments using the latest binary stellar population (BSP) synthesis model and tested the predictions of a recent hierarchical formation model that adopted the new ΛCDM cosmology. The stellar ages and metallicities were estimated from two high-quality published spectra line indices, the Hβ and [MgFe] indices. The results show that the stellar populations of elliptical galaxies are older than 3.9 Gyr and more metal rich than 0.02. Most of our results are in agreement with the model predictions: (1) elliptical galaxies in denser environment are redder and have older populations than field galaxies; (2) elliptical galaxies with more massive stellar components are redder and have older and more metal rich populations than less massive ones; (3) the most massive galaxies have the oldest and most metal rich stars. However, some of our results differ from the model predictions on the metallicity distributions of low- and high-density elliptical galaxies and the dependence on the distance to the cluster center.

Key words: galaxies: stellar content — galaxies: formation — galaxies: elliptical and lenticular, cD

1 INTRODUCTION

Now is a golden era to study galaxy formation and evolution. The elliptical galaxies provide us with a good material for this work because they seem to be homogeneous stellar systems that have uniformly old and red populations and, moreover, they have negligible amounts of gas and have very little on-going star formation. It is therefore convenient to study galaxy formation first via the ellipticals. Significant development in cosmology (e.g. Peebles 1980) has led to the general acceptance of the idea that galaxies were formed in a universe dominated by dark matter, but authors are still arguing about the mechanism of formation of elliptical galaxies: there are two contending views at present: one is that elliptical galaxies formed in a single intense burst of star formation at high redshifts and then their stellar populations just evolved passively to the present day. This "monolithic" scenario can explain the dense cores, metallicity gradients (Kormendy 1987; Thomsen & Baum 1989; Kormendy & Djorgovski 1989) and such fundamental scaling relations as the colour-magnitude relation and as relating to their fundamental planes (Kodama et al. 1998; van Dokkum & Stanford 2003), but it cannot explain the different metallicity levels of halo stars and the large age range of globular clusters. The other view, based on evidence of strong gravitational interactions and mergers between disk galaxies (Toomre & Toomre et al. 1972), is that elliptical galaxies are probably formed by the merging of smaller galaxies: this is known as the "hierarchical" scenario of galaxy formation.

* Supported by the National Natural Science Foundation of China.

In recent years, the hierarchical picture has become increasingly popular, and was extensively simulated, e.g., Kauffmann et al. (1993, 1996, 1998) and the Durham group (Baugh et al. 1996; Baugh et al. 1998; Cole et al. 2000). Some exciting results have emerged in these studies, e.g. the star formation histories of galaxies (see Baugh et al. 1998). Observational studies, however, showed some unexpected trends: First, it was found that a significant fraction of early-type galaxies are formed recently (Barger et al. 1996). Secondly, it was found that only a small fraction of mass is involved in the interaction and merger of galaxies. Thirdly, some related issues, e.g. the supra-solar [α/Fe] ratio of massive ellipticals suggest that these galaxies formed on relatively short time-scales and have an initial mass function that is skewed towards massive stars. It seems that these observed trends are difficult to explain on the early hierarchical models (Thomas 1999). De Lucia et al. (2006) put forth a new hierarchical model, which, adopting the new ΛCDM cosmology and using high-resolution simulation, tried to explain the "anti-hierarchical" behavior of star formation in elliptical galaxy population and made some new predictions. It seems worthwhile to pursue this new hierarchical model further.

Because different galaxy formation models usually predict different histories of star formation, the techinque of stellar population synthesis has become a very useful and popular technique in recent years in the study of galaxy formation. A series of detailed studies of stellar populations of galaxies, both observational and semi-analytical, have been carried out (e.g. Trager et al. 2000a, b; Terlevich & Forbes 2002; van Zee et al. 2004). However, all these works used single stellar population (SSP) synthesis models (e.g. Vazdekis et al. 1996, 1997; Vazdekis 1999; Worthey 1994; Bruzual & Charlot (2003) when the binary stellar population (BSP) synthesis model was not available. However, as pointed out by Zhang et al. (2005a, b), binary interaction plays an important role in the evolutionary population synthesis and gives different results from SSP models (see Zhang 2005a for more detail). Thus we now ask the question: how will the hierarchical formation model of elliptical galaxies be supported if we take the binary interaction in stellar population synthesis into account ? In this paper we attempt an answer with the BSP model of Zhang et al. (2005b) and the hierarchical formation model of De Lucia et al. (2006) while leaving the investigation of the very complicated effects of binary interaction to another paper. The structure of this paper is as follows. In Section 2 we introduce our galaxy sample and the BSP model. In Section 3 we give a description of the determination of stellar ages and metallicities and then show the main results. In Section 4 we test the latest hierarchical model of the formation of elliptical galaxies and finally we give a discussion and our conclusions in Section 5.

2 THE DATA SAMPLE AND BSP MODEL

2.1 The Galaxy Sample

Our main sample consists of all the normal ellicptical galaxies in the sample of Thomas et al. (2005). Thus, it includes 71 normal elliptical galaxies, while excluding 51 S0 and 2 cD galaxies. The $B-V$ colors and B-band absolute magnitudes of these ellipticals are supplemented from the HyperLeda database (*http://www.brera.mi.astro.it/hypercat/*) wherever possible. Of our 71 ellipticals, 42 reside in low-density, and 29 in high-density environments. In fact, these data are very good for estimating stellar ages and metallicities because they were selected from some creditable sources (González 1993; Mehlert et al. 2000, 2003; Beuing et al. 2002; Lauberts & Valentijn 1989) and reobserved by Thomas et al. if necessary (19 objects were reobserved). In particular, because the absorption-line strengths of galaxies are measured as functions of the galaxy radius, we can adopt the "central" line indices measured within one-tenth of the effective radius r_e, so that our analysis is free of any aperture effects. We use the Lick line indices Hβ, Mgb, and $\langle$Fe$\rangle$ = 0.5$\times$ (Fe 5270+Fe 5335) directly. According to Thomas et al. (2005), the median 1σ errors in Hβ, Mgb, Fe 5270 and Fe 5335 are 0.06, 0.06, 0.07 and 0.08, respectively. There is also another advantage in the data: the elliptical galaxies span a large range in the central velocity dispersion: $0 \leq \sigma_0$/(km s^{-1}) $\leq$340, which is very convenient when studying the relations between the mass and the other parameters, following Thomas et al. (2005). Table 1 lists successively the galaxy's name, velocity dispersion, the line widths of Hβ, Mgb, $\langle$Fe$\rangle$, together with their observational uncertainties, M_B, $B-V$, and whether the environment E is low (L) or high (H) density. Our sample also includes 11 elliptical galaxies in the Fornax cluster from Kuntschner (2000), but they are only used for testing the predictions relating to dependence on the distance to the cluster center.

Table 1 Data of ellipticals in low (L) and high (H) environments (E) (σ_0 denotes the velocity dispersion, all the line indices are within the r_e/10 aperture).

Name	σ_0 [km s^{-1}]	Hβ [Å]	δHβ [Å]	Mgb [Å]	δMgb [Å]	$\langle$Fe$\rangle$ [Å]	$\delta\langle$Fe$\rangle$ [Å]	M_B [mag]	$B-V$ [mag]	E
NGC 0221	72.1	2.31	0.05	2.96	0.03	2.75	0.03	–17.424	0.800	L
NGC 0315	321.0	1.74	0.06	4.84	0.05	2.88	0.05	–22.472	0.929	L
NGC 0507	262.2	1.73	0.09	4.52	0.11	2.78	0.10	–22.121	0.888	L
NGC 0547	235.6	1.58	0.07	5.02	0.05	2.82	0.05	–21.663		L
NGC 0636	160.3	1.89	0.04	4.20	0.04	3.03	0.04	–19.798	0.908	L
NGC 0720	238.6	1.77	0.12	5.17	0.11	2.87	0.09	–20.786	0.948	L
NGC 0821	188.7	1.66	0.04	4.53	0.04	2.95	0.04	–20.753	0.865	L
NGC 1453	286.5	1.60	0.06	4.95	0.05	2.98	0.05	–21.613	0.911	L
NGC 1600	314.8	1.55	0.07	5.13	0.06	3.06	0.06	–22.419	0.923	L
NGC 1700	227.3	2.11	0.05	4.15	0.04	3.00	0.04	–21.903	0.890	L
NGC 2300	251.8	1.68	0.06	4.98	0.05	2.97	0.05	–20.754	0.966	L
NGC 2778	154.4	1.77	0.08	4.70	0.06	2.85	0.05	–19.206	0.889	L
NGC 3377	107.6	2.09	0.05	3.99	0.03	2.61	0.03	–19.169	0.820	L
NGC 3379	203.2	1.62	0.05	4.78	0.03	2.86	0.03	–20.608	0.927	L
NGC 3608	177.7	1.69	0.06	4.61	0.04	2.94	0.04	–19.733	0.909	L
NGC 3818	173.2	1.71	0.08	4.88	0.07	2.97	0.06	–19.400	0.908	L
NGC 4278	232.5	1.56	0.05	4.92	0.04	2.68	0.04	–19.359	0.895	L
NGC 5638	154.2	1.65	0.04	4.64	0.04	2.84	0.04	–19.974	0.892	L
NGC 5812	200.3	1.70	0.04	4.81	0.04	3.06	0.04	–20.450	0.927	L
NGC 5813	204.8	1.42	0.07	4.65	0.05	2.67	0.05	–21.113	0.916	L
NGC 5831	160.5	2.00	0.05	4.38	0.04	3.05	0.03	–19.813	0.897	L
NGC 6127	238.9	1.50	0.05	4.96	0.06	2.85	0.05	–21.352	0.944	L
NGC 6702	173.8	2.46	0.06	3.80	0.04	3.00	0.04	–21.613	0.839	L
NGC 7052	273.8	1.48	0.07	5.02	0.06	2.84	0.05	–21.199		L
NGC 7454	106.5	2.15	0.06	3.27	0.05	2.48	0.04	–19.930	0.866	L
NGC 7785	239.6	1.63	0.06	4.60	0.04	2.91	0.04	–21.375	0.949	L
ESO 107–04	147.0	2.24	0.25	3.63	0.16	2.97	0.09	–20.386	0.849	L
ESO 148–17	134.5	2.26	0.52	3.49	0.32	2.58	0.20	–19.865	0.875	L
IC 4797	220.6	1.92	0.26	4.52	0.18	2.75	0.10	–20.876	0.908	L
NGC 0312	254.8	1.83	0.09	4.56	0.08	2.48	0.05	–21.937	0.929	L
NGC 0596	161.8	2.12	0.05	3.95	0.04	2.81	0.03	–20.424	0.845	L
NGC 0636	178.5	1.86	0.26	4.38	0.17	2.83	0.09	–19.798	0.908	L
NGC 1052	202.6	1.22	0.04	5.53	0.03	2.77	0.02	–20.139	0.900	L
NGC 1395	250.0	1.62	0.05	5.21	0.04	2.93	0.03	–21.211	0.921	L
NGC 1407	259.7	1.67	0.07	4.88	0.06	2.85	0.03	–21.432	0.946	L
NGC 1549	203.3	1.79	0.03	4.39	0.03	2.88	0.02	–19.981	0.906	L
NGC 2434	180.4	1.87	0.13	3.72	0.10	2.87	0.07	–19.828	0.818	L
NGC 2986	282.2	1.48	0.06	4.97	0.05	2.92	0.03	–21.064	0.891	L
NGC 3078	268.1	1.12	0.09	5.20	0.07	3.16	0.04	–20.893	0.916	L
NGC 3923	267.9	1.87	0.08	5.12	0.07	3.07	0.04	–21.151	0.906	L
NGC 5791	271.8	1.60	0.19	5.06	0.15	3.30	0.10	–21.123	0.89	L
NGC 5903	209.2	1.68	0.10	4.44	0.08	2.90	0.05	–21.220	0.839	L
NGC 4261	288.3	1.34	0.06	5.11	0.04	3.01	0.04	–21.299	0.952	H
NGC 4374	282.1	1.51	0.04	4.78	0.03	2.82	0.03	–20.888	0.931	H
NGC 4472	279.2	1.62	0.06	4.85	0.06	2.91	0.05	–21.785	0.928	H
NGC 4478	127.7	1.84	0.06	4.33	0.06	2.94	0.05	–19.564	0.873	H
NGC 4489	47.2	2.39	0.07	3.21	0.06	2.66	0.05	–18.189	0.804	H
NGC 4552	251.8	1.47	0.05	5.15	0.03	2.99	0.03	–20.798	0.936	H
NGC 4697	162.4	1.75	0.07	4.08	0.05	2.77	0.04	–21.239	0.869	H
NGC 7562	248.0	1.69	0.05	4.54	0.04	2.87	0.04	–21.416	0.938	H
NGC 7619	300.3	1.36	0.04	5.06	0.04	3.06	0.04	–21.973	0.925	H
NGC 7626	253.1	1.46	0.05	5.05	0.04	2.83	0.04	–21.673	0.947	H
NGC 4839	275.5	1.42	0.04	4.92	0.04	2.75	0.04	–22.263	0.879	H
NGC 4841A	263.9	1.53	0.05	4.51	0.05	2.89	0.04	–21.380		H
NGC 4926	273.3	1.50	0.06	5.17	0.06	2.50	0.05	–21.443	0.954	H
IC 4051	258.7	1.42	0.06	5.34	0.07	2.75	0.05	–20.204	0.933	H
NGC 4860	280.5	1.39	0.06	5.39	0.07	2.85	0.05	–20.948	0.973	H
NGC 4923	186.0	1.70	0.05	4.43	0.05	2.69	0.04	–19.983	0.888	H
NGC 4840	216.6	1.63	0.07	4.94	0.07	2.91	0.06	–20.131	0.954	H
NGC 4869	188.1	1.40	0.05	4.83	0.05	2.90	0.04	–20.797	0.934	H
NGC 4908	192.4	1.58	0.09	4.58	0.09	2.65	0.07	–21.075	0.936	H

Table 1 – Continued.

Name	σ_0 [km s^{-1}]	Hβ [Å]	δHβ [Å]	Mgb [Å]	δMgb [Å]	$\langle$Fe$\rangle$ [Å]	$\delta\langle$Fe$\rangle$ [Å]	M_B [mag]	$B-V$ [mag]	E
IC 4045	167.3	1.46	0.06	4.70	0.07	2.77	0.05	–20.282	0.943	H
NGC 4850	155.8	1.57	0.06	4.39	0.06	2.58	0.05	–19.601	0.956	H
NGC 4872	171.7	2.05	0.05	4.05	0.06	2.82	0.04	–20.893	0.874	H
NGC 4957	208.4	1.76	0.03	4.53	0.03	2.93	0.02	–21.177	0.925	H
NGC 4952	252.6	1.71	0.03	4.76	0.03	2.69	0.02	–21.203		H
GMP 1990	208.9	1.40	0.04	4.78	0.04	2.50	0.03			H
NGC 4827	243.7	1.53	0.03	4.89	0.03	2.80	0.02	–21.495	0.904	H
NGC 4807	178.5	1.81	0.06	4.39	0.06	2.78	0.05	–20.703	0.919	H
ESO 185–54	277.2	1.57	0.06	5.11	0.05	3.07	0.03	–21.861		H
NGC 3224	155.8	2.31	0.14	3.91	0.12	2.92	0.08	–20.508	0.828	H

2.2 The BSP Model

In this work, we translate the central line indices into the stellar ages and metallicities via the BSP model of Zhang et al. (2005b). This model provides high-resolution (0.3 Å) absorption-lines defined by the Lick Observatory Image Dissector Scanner (Lick/IDS) system for an extensive set of instantaneous burst binary stellar populations with binary interactions. In particular, its stellar populations span an age range 1–15 Gyr and a metallicity range 0.0001–0.03.

3 STELLAR AGES AND METALLICITIES OF ELLIPTICAL GALAXIES

To determine the BSP equivalent stellar ages and metallicities, we use the Hβ and [MgFe] line indices (González 1993). The latter is defined as $\sqrt{\mathrm{Mgb}\times 0.5\times(\mathrm{Fe}\,5270+\mathrm{Fe}\,5335)}$. Figure 1 displays the Hβ vs. [MgFe] plot for the 71 elliptical galaxies superimposed on the model constant age and metallicity curves. The open and filled circles represent ellipticals in low- and high-density environments, respectively, and their observational error bars are drawn.

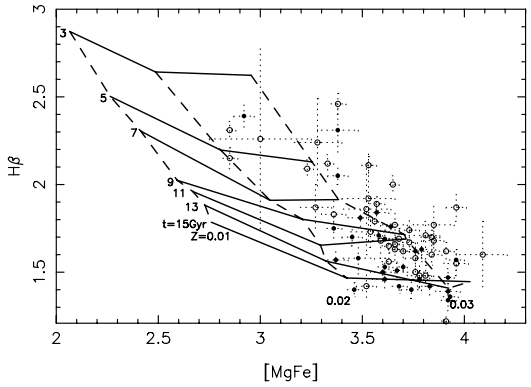

Fig. 1 Plot of line-strength indices in the central r_e/10 aperture of the sample elliptical galaxies in low-density environments (open circles) and high-density environments (filled circles). Observational error bars are shown. Solid and dashed lines are, respectively, lines of constant age (isochrones) and constant metallicity (isofers) in the BSP model.

The BSP-equivalent stellar age and metallicity of each elliptical galaxy is determined by the best-fitting point in an age (t)–metallicity (Z) grid. which was made sufficiently fine by interpolating the BSP model values at intervals $\Delta t = 0.1$ Gyr and $\Delta Z = 0.0001$. The best-fitting (t, Z) was found by a maximum-likelihood fitting, specifically, by minimizing the function,

$$\chi^2(t_i, Z_i) = (\mathrm{H}\beta_i - \mathrm{H}\beta_\mathrm{o})^2 + ([\mathrm{MgFe}]_i - [\mathrm{MgFe}]_\mathrm{o})^2, \quad (1)$$

Table 2 Stellar ages, metallicities and associated 1σ uncertainties of 71 sample elliptical galaxies. The stellar ages and their uncertainties are in Gyr.

Name	Age	Z	Name	Age	Z
NGC 0221	4.3 ± 0.3	0.0230 ± 0.0008	NGC 2434	8.3 ± 5.9	0.0234 ± 0.0041
NGC 0315	9.0 ± 2.1	≥ 0.03	NGC 2986	12.6 ± 2.0	0.0284 ± 0.0011
NGC 0507	9.2 ± 2.3	0.0268 ± 0.0023	NGC 3078	13.9 ± 0.5	≥ 0.03
NGC 0547	11.8 ± 2.7	0.0286 ± 0.0025	NGC 3923	9.0 ± 2.5	≥ 0.03
NGC 0636	7.8 ± 0.2	≥ 0.03	NGC 5791	$\geq 15 \pm 3.2$	≥ 0.03
NGC 0720	11.2 ± 2.2	≥ 0.03	NGC 5903	10.3 ± 4.1	0.0276 ± 0.0040
NGC 0821	11.2 ± 1.7	0.0280 ± 0.0012	NGC 4261	13.0 ± 0.3	$\geq 0.03 \pm 0.0004$
NGC 1453	11.7 ± 0.3	$\geq 0.03 \pm 0.0006$	NGC 4374	13.3 ± 0.6	0.0256 ± 0.0004
NGC 1600	14.0 ± 2.0	0.0286 ± 0.0014	NGC 4472	11.4 ± 2.6	0.0296 ± 0.0032
NGC 1700	6.0 ± 0.1	≥ 0.03	NGC 4478	7.9 ± 0.7	$\geq 0.03 \pm 0.0017$
NGC 2300	11.4 ± 0.2	≥ 0.03	NGC 4489	3.9 ± 0.3	0.0254 ± 0.0012
NGC 2778	8.6 ± 1.0	$\geq 0.03 \pm 0.0010$	NGC 4552	14.3 ± 1.8	0.0285 ± 0.0014
NGC 3377	5.4 ± 0.4	0.0283 ± 0.0011	NGC 4697	9.3 ± 1.1	0.0229 ± 0.0014
NGC 3379	11.5 ± 2.7	0.0281 ± 0.0027	NGC 7562	9.7 ± 1.7	0.0283 ± 0.0017
NGC 3608	9.6 ± 1.8	0.0298 ± 0.0017	NGC 7619	13.0 ± 0.4	$\geq 0.03 \pm 0.0003$
NGC 3818	11.2 ± 2.2	≥ 0.03	NGC 7626	13.2 ± 0.8	0.0274 ± 0.0007
NGC 4278	12.3 ± 2.2	0.0258 ± 0.0023	NGC 4839	≥ 15.0	0.0242 ± 0.0007
NGC 5638	11.3 ± 1.6	0.0272 ± 0.0015	NGC 4841A	12.6 ± 2.3	0.0252 ± 0.0020
NGC 5812	11.3 ± 0.2	≥ 0.03	NGC 4926	12.9 ± 2.1	0.0246 ± 0.0018
NGC 5813	$\geq 15 \pm 0.1$	0.0217 ± 0.0009	IC 4051	13.0 ± 0.6	0.0285 ± 0.0009
NGC 5831	8.0 ± 0.2	≥ 0.03	NGC 4860	13.0 ± 2.0	$\geq 0.03 \pm 0.0018$
NGC 6127	13.5 ± 1.1	0.0268 ± 0.0019	NGC 4923	9.8 ± 4.0	0.0247 ± 0.0031
NGC 6702	4.0 ± 0.0	≥ 0.03	NGC 4840	11.4 ± 0.5	$\geq 0.03 \pm 0.0012$
NGC 7052	12.7 ± 2.0	0.0278 ± 0.0010	NGC 4869	13.0 ± 2.0	0.0272 ± 0.0027
NGC 7454	5.3 ± 0.8	0.0200 ± 0.0021	NGC 4908	12.4 ± 2.5	0.0234 ± 0.0022
NGC 7785	11.4 ± 2.6	0.0276 ± 0.0031	IC 4045	$\geq 15 \pm 0.3$	0.0230 ± 0.0010
ESO 107–04	4.6 ± 1.6	$\geq 0.03 \pm 0.0022$	NGC 4850	12.8 ± 2.1	0.0210 ± 0.0016
ESO 148–17	4.5 ± 8.6	0.0255 ± 0.0109	NGC 4872	5.8 ± 0.2	≥ 0.03
IC 4797	7.6 ± 6.3	$\geq 0.03 \pm 0.0067$	NGC 4957	8.6 ± 0.3	0.0297 ± 0.0007
NGC 0312	8.5 ± 1.6	0.0246 ± 0.0048	NGC 4952	9.4 ± 1.1	0.0275 ± 0.0005
NGC 0596	5.3 ± 0.2	≥ 0.03	GMP 1990	≥ 15.0	0.0206 ± 0.0006
NGC 0636	7.7 ± 4.4	0.0299 ± 0.0056	NGC 4827	12.4 ± 1.2	0.0268 ± 0.0012
NGC 1052	13.0 ± 0.0	≥ 0.03	NGC 4807	8.4 ± 0.8	0.0274 ± 0.0023
NGC 1395	11.8 ± 0.2	≥ 0.03	ESO 185-54	12.0 ± 2.0	$\geq 0.03 \pm 0.0012$
NGC 1407	11.1 ± 2.1	$\geq 0.03 \pm 0.0015$	NGC 3224	4.4 ± 0.9	≥ 0.03
NGC 1549	8.5 ± 0.4	0.0283 ± 0.0010			

where $\mathrm{H}\beta_i$ and $[\mathrm{MgFe}]_i$ are the $\mathrm{H}\beta$ and [MgFe] indices corresponding to the ith BSP model grid point, and $\mathrm{H}\beta_\mathrm{o}$ and $[\mathrm{MgFe}]_\mathrm{o}$ are the observed indices. We also calculated the associated uncertainties by searching best-fitting (t, Z)s for [$\mathrm{H}\beta_\mathrm{o}$–error, $[\mathrm{MgFe}]_\mathrm{o}$], [$\mathrm{H}\beta_\mathrm{o}$+error, $[\mathrm{MgFe}]_\mathrm{o}$], [$\mathrm{H}\beta_\mathrm{o}$, $[\mathrm{MgFe}]_\mathrm{o}$–error] and [$\mathrm{H}\beta_\mathrm{o}$, $[\mathrm{MgFe}]_\mathrm{o}$+error], respectively, and then take their deviations from the best-fitting (t, Z) derived from [$\mathrm{H}\beta_\mathrm{o}$, $[\mathrm{MgFe}]_\mathrm{o}$]. Although the four pairs of (t, Z) derived by the search do not describe completely the total range of possible age and metallicity values inside the 1σ error ellipse, the maximum deviations of stellar age and metallicity can provide us with a sufficient idea of the uncertainties involved when translating the errors in the $\mathrm{H}\beta$-[MgFe] plane to the errors in t and Z (Denicoló et al. 2005), and we took the maximum deviation as the associated 1σ uncertainty in the stellar age and metallicity. Table 2 lists the stellar ages, metallicities and their 1σ uncertainties of the main sample. The stellar ages of these ellipticals range from 3.9 Gyr to older than 15 Gyr and the stellar metallicities range from 0.02 to richer than 0.03. It seems that the ages do not vary as widely as was found by Trager et al. (2000a) (1.5–18 Gyr). This is probably due to the different stellar population synthesis model we used. It is found that about 78% of the elliptical galaxies have stellar populations older than 8 Gyr. The average stellar age is 10.37 Gyr and the average metallicity is 0.0277. The average 1σ uncertainties are, respectively, 1.58 Gyr and 0.0015,

4 TEST OF THE NEW HIERARCHICAL MODEL

The hierarchical formation of elliptical galaxies has been simulated either with N-body simulation or with semi-analytic simulation. Different models based on cosmologies with the critical matter density have usu-

ally given different predictions of stellar properties. The cosmologies used before have now been replaced by the ΛCDM scenario. Based on this scenario, De Lucia et al. (2006) constructed a new hierarchical formation model of elliptical galaxies and studied how their history of star formation and their age and metallicity depend on the environment and on the stellar mass. They made some pecific predictions: 1) the ellipticals in high-density environments should be older, more metal rich and redder than the field ellipticals. 2) The most massive elliptical galaxies should have the oldest and most metal rich stellar populations. 3) The stellar age, metallicity and galaxy color should increase with increasing the stellar mass. 4) The stellar mass, age, metallicity and color of an elliptical galaxy in a cluster of galaxies should, on average, decrease with increasing distance from the cluster center. In addition, the model quantified the effective progenitors of ellipticals as a function of present stellar mass and then predicted the "down-sizing" or "anti-hierarchical trend" of star formation history of ellipticals in a ΛCDM universe. The model is important, because if it is right, then we will have a much better understanding of the formation of elliptical galaxies. Therefore, it is very necessary to test this model. Of course, taking the binary interaction into to the test is important because more than half of stars are binaries as we know. The detailed tests are as follows.

4.1 Variations of Age, Metallicity and Color with Environment

A basic prediction of the hierarchical galaxy formation scenario is that more massive galaxies have, on average, older stellar populations than less massive galaxies (e.g. Kauffmann 1996). This is also predicted by the model of De Lucia et al. (2006). De Lucia et al.'s model predicted furthermore that galaxies in higher density environments should have more metal rich and redder populations than those in lower density environments, due to the formation of higher density regions from the density peaks in the primordial field of density fluctuations. Here we test these specific predictions with our data.

Figure 2 displays the histograms of stellar age distribution of both the low-density ellipticals (dashed) and the high-density ellipticals (solid). We see that the high-density ellipticals indeed have an older stellar population than the low density ellipticals, older by 1.47 Gyr on average.

In Figure 3 we show the stellar metallicity distributions of low and high-density ellipticals. As can be seen, the plot shows that, compared to the low-density ellipticals (dahsed line), the high-density ellipticals (solid line) do NOT have a more metal rich stellar population. We also can see this feature clearly in Figure 1, namely, ellipticals in high-density environment (filled circles) are in fact distributed in a lower metallicity region than the field ellipticals (unfilled circles).

Our result on the $B-V$ color distributions of the two types of elliptical galaxies is consistent with the De Lucia (2006) model. See Figure 4. On average, the high-density ellipticals are about 0.02 mag redder than the low-density ones.

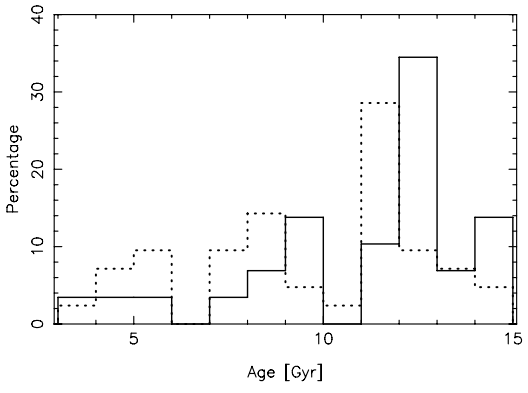

Fig. 2 Stellar age distributions of low-density elliptical (dashed line) and high-density ellipticals (solid line).

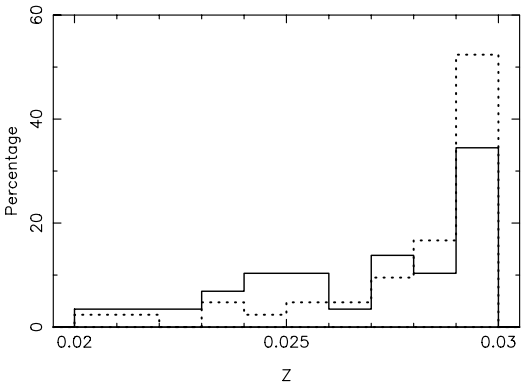

Fig. 3 Histograms of stellar metallicity distribution of low-density ellipticals (dashed line) and high-density ellipticals (solid line).

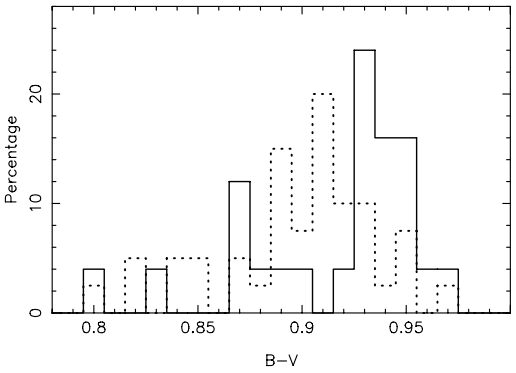

Fig. 4 $B-V$ distributions of low-density ellipticals (dashed line) and high-density ellipticals (solid line).

4.2 Stellar Age, Metallicity and Galaxy Color Variation with Stellar Mass

While the most important result and prediction of the De Lucia model is that the most massive elliptical galaxies have the oldest and most metal rich stellar populations, the model also predicts that the stellar age, metallicity and galaxy color should increase with increasing stellar mass. We test these predictions in Figures 5, 6 and 7. Here the stellar mass M_* of the elliptical galaxy is calculated from its velocity dispersion σ_0 according to the formula given by Thomas et al. (2005):

$$\log(M_*/M_\odot) = 0.63 + 4.52\log(\sigma_0/(\mathrm{km\ s^{-1}}))\,. \tag{2}$$

According to previous studies, there is usually a relation between the mass and luminosity of elliptical galaxies, e.g. $(M/L)_B = (5.93 \pm 0.25)h_{50}$ (van der Marel 1991). It means that more luminous elliptical galaxies have greater masses. Therefore the absolute magnitude is usually used as a mass indicator (e.g. Terlevich & Forbes 2002). We compared the masses calculated above with the absolute B-band magnitudes taken from HyperLeda database *(http://www.brera.mi.astro.it/hypercat/)*, and we found that the more luminous elliptical galaxies indeed have greater masses. Thus, as a whole, the stellar masses estimated from the fitting function can be taken as representing the real stellar masses of elliptical galaxies.

In Figure 5 the stellar age is plotted as a function of the stellar mass. The filled squares with error bars are look-back times and stellar masses predicted by the De Lucia model. The look-back time of a galaxy is the time corresponding to the redshift when 50 percent of its stars were formed. Open and filled circles with arrows show galaxies that have stellar ages possibly older than 15 Gyr (the maximum age of the BSP model). It is easy to see a trend that more massive ellipticals have older stellar populations and that the most massive galaxies have the oldest stars, but the change of stellar age with stellar mass is different from the model prediction. This may be caused by the somewhat different definitions of look-back time and stellar age. Specifically, the stellar age in the simple BSP model is defined corresponding to the redshift when all the stars formed. When we fit the relation between stellar age and stellar mass, we find a linear relation: age = $3.115\log(M_*/M_\odot) - 24.147$, with a correlation coefficient of 0.656.

In Figure 6, we show the stellar metallicity – stellar mass relation of the main sample elliptical galaxies. The open and filled circles with arrows are ellipticals that have populations possibly more metal rich than 0.03 (the maximum metallicity of the BSP model). The open pentacles with dashed error bars represent the predictions of the De Lucia model. From this plot, we see that all galaxies have metallicities richer than the predictions of the De Lucia model. However, if we only consider ellipticals with metallicities below 0.03, then our data can be expressed by a trend similar to the prediction of the De Lucia model, with the addition of a constant 0.074 (the difference in maximum metallicity between the De Lucia model and the BSP model) to each De Luca predicted metallicity. We plot the trend with filled pentacles with solid error bars in Figure 7. It means that our data show the same trend as the De Lucia model and the difference between our data and the model prediction is possibly due to some limits in the model.

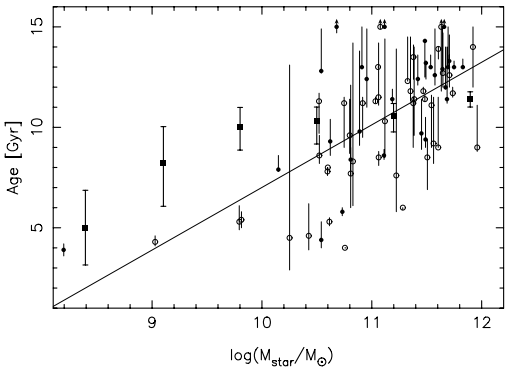

Fig. 5 Stellar age - mass relation for 71 elliptical galaxies. Filled squares with error bars are predictions of the galaxy formation model. Arrows indicate galaxies that have stellar populations possibly older than the maximum age of the BSP model (15 Gyr). Solid line is the least-squares fit to the data. Open and filled circles represent low- and high-density ellipticals, respectively.

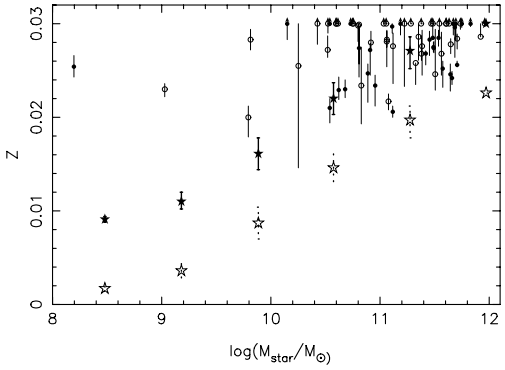

Fig. 6 Stellar metallicity – mass relation of our sample elliptical galaxies. Arrows indicate galaxies that have stellar metallicities larger than the maximum metallicity available for the BSP model (0.03). The open pentacles with dashed error bars represent the predictions of the De Lucia model and the filled pentacles with solid error bars are the same with a constant 0.074 added. The open and filled circles have the same meanings as in Fig. 5.

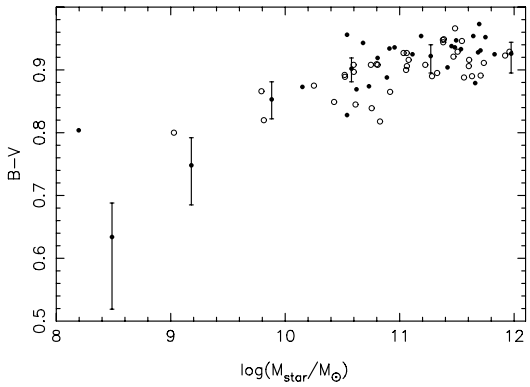

Fig. 7 $B-V$ and stellar mass relation of the sample elliptical galaxies. The masses are calculated from Equation (2) . Filled squares with error bars represent the values predicted by the model. Open and filled circles have the same meanings as in Fig. 5.

The relation between galaxy color and stellar mass is plotted in Figure 7. The stellar masses are calculated by Equation (2). Filled and open circles represent ellipticals in high-density and low-density environments. Filled squares with error bars mark the color – stellar mass relation predicted by the model. We see that the model agrees well with our data.

4.3 Variation of Stellar Age, Metallicity, Mass and Color with Distance to the Cluster-Centre

The De Lucia model predicted a clear trend driven by mass segregation and incomplete mixing of the galaxy population during the cluster assembly. According to the prediction, within a given cluster, the stellar masses, ages, metal abundances and galaxy colors should, on average, decrease with increasing distance from the cluster center. To test these predicted trends, we selected 11 elliptical galaxies of Fornax cluster and determined their stellar ages and metallicities from the Hβ and [MgFe] line indices within r $_e$/8, taken from Kuntschner (2000). Their coordinates and $B-V$ colors are taken from the HyperLeda database.

Table 3 shows the main data of the 11 ellipticals. It should be noted that we use the angular distance rather than the linear distance to the central galaxy NGC 1399 (a galaxy well studied, e.g. Loewenstein et al. 2005), which is difficult to determine from the individual distances affected by uncertain peculiar velocities. The main results are shown in Figures 8, 9 and 10.

Table 3 Main data for 11 member elliptical galaxies of the Fornax cluster (log M_* is the logarithm of the stellar mass and θ_{1399} is the angular distance to NGC 1399).

Name	$\log(M_*/M_\odot)$	θ_{1399} [arcmin]	$B-V$ [mag]	Age [Gyr]	Z
NGC 1336	9.5886	0.324	0.809	14.6 ± 4.9	0.0179 ± 0.0029
NGC 1339	10.5695	3.318	0.903	13.8 ± 2.4	0.0270 ± 0.0030
NGC 1351	10.5559	0.636	0.844	14.8 ± 2.9	0.0235 ± 0.0039
NGC 1373	9.1050	0.294	0.832	8.6 ± 1.9	0.0212 ± 0.0038
NGC 1374	10.8768	0.240	0.894	11.8 ± 2.3	0.0299 ± 0.0041
NGC 1379	10.1853	0.036	0.866	9.8 ± 4.7	0.0241 ± 0.0039
NGC 1399	12.2645	0	0.934	14.1 ± 0.9	≥ 0.03
NGC 1404	11.5458	0.150	0.941	$\geq 15 \pm 3.0$	≥ 0.03
NGC 1419	9.9774	2.160	0.863	14.9 ± 2.8	0.0159 ± 0.0034
NGC 1427	10.7684	0.084	0.885	11.1 ± 3.0	0.0262 ± 0.0034
IC 2006	10.2757	0.588	0.896	13.7 ± 1.0	0.0294 ± 0.0010

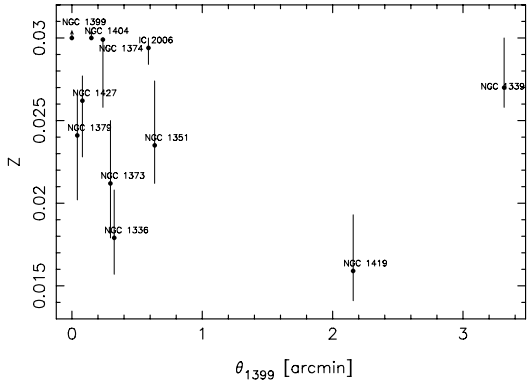

Fig. 8 Plot of stellar metallicity Z versus angular distance to NGC 1399, θ_{1399}.

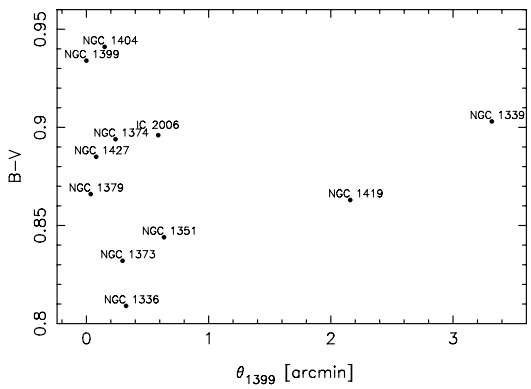

Fig. 9 Plot of $B-V$ versus θ_{1399}.

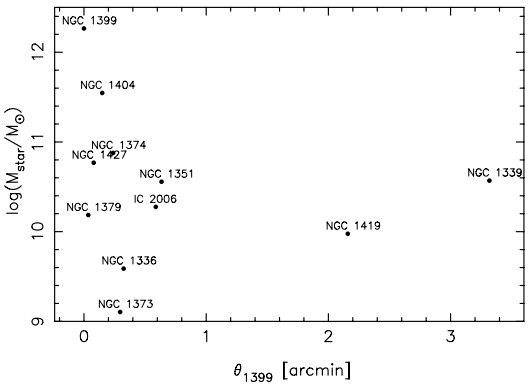

Fig. 10 Plot of $[\log(M_{\rm star}/M_\odot)$ versus $\theta_{1399}]$.

In Figure 8, the stellar metallicity is plotted against the angular distance to NGC1399. We see that it is difficult to find a clear trend over the whole angular distance range. However, over a limited range, e.g. 2.5 arcmin, the stellar metallicity seems to decrease with increasing angular distance.

The relation between the $B-V$ color and the angular distance is shown in Figure 9 and that between the stellar mass and angular distance, in Figure 10. These two plots do not seem to show the trend predicted by the model, nor do they show an opposite trend. Incidentally, we found that the plot between the stellar age and mass (not shown here) to be almost random.

In Figures 8, 9 and 10, there are only three galaxies with angular distances farther than 0.6 arcmin, and we think the smaller elliptical galaxies located farther than 0.6 arcmin must have a bearing on any such distance dependence. Furthermore, our results may have been affected by the small size of our sample.

5 DISCUSSION AND CONCLUSIONS

We determined the stellar ages and metallicities of about 80 elliptical galaxies using the BSP model of Zhang et al. (2005b) and tested, for the first time, the predictions of the latest model of formation of elliptical galaxies (De Lucia 2006). We found that elliptical galaxies have stellar populations that are about 10 Gyr old and are more metal rich than 0.02 (see also Zhou et al. 1992).

In our analysis of the data, we found that the stellar populations of elliptical galaxies in high-density environment are about 1.5 Gyr older, and 0.001 less metal rich, than those of the field elliptical galaxies. We also found that elliptical galaxies in high-density environment are about 0.02 mag redder than the field ellipticals. Furthermore, we found that the more massive ellipticals are redder and have older and more metal rich stellar populations than the less massive ones. It also seems that the most massive ellipticals have the oldest and most metal rich populations. However, elliptical galaxies in low-density environment show more metal rich stellar populations than those in high-density environment: this trend is directly opposite to the prediction of the model of De Lucia et al. (2006). When we tested the dependence of the stellar mass, age, metallicity and galaxy color on the distance to the cluster center, our results do not show any clear support nor opposition to the model predictions, and it seems that our results are affected by using the angular distance instead of the linear distance and by the small size of our sample. In summary, the results derived from the BSP model support the ΛCDM-based hierarchical model of elliptical galaxies formation, except the dependence of the metallicity on the environment and the variations with the distance to the cluster center. The doubtless conflict between our result and the prediction of the model, as regards the dependence of metallicity on the environment, should be noted.

Acknowledgements We thank the HyperLeda team for supplying us with the photometry of galaxies on the internet: *http://www.brera.mi.astro.it/hypercat/*. We also thank Profs. Xu Zhou, Tinggui Wang and Tao Kiang for useful discussion and improving the presentation in English. This work is supported by the National Natural Science Foundation of China (Grant Nos. 10433030, 10521001 and 10303006), the Chinese Academy of Sciences (No. KJX2-SW-T06) and Yunnan Natural Science Foundation (Grant No. 2005A0035Q).

References

Barger A. J., Aragon-Salamanca A., Ellis R. S., Couch W. J., Smail I., Sharples R. M., 1996, MNRAS, 279, 1
Baugh C. M., Cole S., Frenk C. S., Lacey C. G., 1998, ApJ, 498, 504
Baugh C. M., Cole S., Frenk C. S., 1996, MNRAS, 283, 1361
Beuing J., Bender R., Mendes de Oliveira C., Thomas D., Maraston C., 2002, A&A, 395, 431
Bruzual G., Charlot S., 2003, MNRAS, 344, 1000
Cole S., Lacey C. G., Baugh C. M. et al., 2000, MNRAS, 319, 168
De Lucia G., Springel V., White S. D. M. et al., 2006, MNRAS, 366, 499
Denicoló G., Terlevich R., Terlevich E. et al., 2005, MNRAS, 358, 813
González J., 1993, Ph.D. thesis, Univ. California, Santa Cruz
Kauffmann G., White S. D. M., Guiderdoni B., 1993, MNRAS, 264, 201
Kauffmann G., 1996, MNRAS, 281, 487
Kauffmann G., Charlot S., 1998, MNRAS, 294, 705
Kodama T., Arimoto N., Barger A.J., Aragón-Salamanca A., 1998, A&A, 334, 99

Kormendy J., 1987, In: S. M. Faber, ed., Nearly Normal Galaxies: From the Planck Time to the Present, New York: Springer-Verlag, 81
Kormendy J., Djorgovski S., 1989, ARA&A, 27, 235
Kuntschner H., 2000, MNRAS, 315, 184
Lauberts A., Valentijn E. A., 1989, The Surface Photometry Catalogue of the ESO-Upsalla Galaxies, Garching: ESO
Loewenstein M., Angelini L., Mushotzky R. F., 2005, ChJAA, 5s, 159
Mehlert D., Saglia R. P., Bender R., Wegner G., 2000, A&AS, 141, 449
Mehlert D., Thomas D., Saglia R. P. et al., 2003, A&A, 407, 423
Peebles P. J. E., 1980, The Large-Scale Structure of the Universe, Princeton: Princeton University Press
Terlevich A. I., Forbes D., 2002, MNRAS, 330, 547
Thomas D., 1999, MNRAS,306, 655
Thomas D., Maraston C., Bender R. et al., 2005, ApJ, 621, 673
Thomsen B., Baum W. A., 1989, ApJ, 347, 214
Toomre A., Toomre J., 1972, ApJ, 178, 623
Trager S. C., Faber S. M., Worthey G., González J. J., 2000a, AJ, 119, 1645
Trager S. C., Faber S. M., Worthey G., González J. J., 2000b, AJ, 120, 165
van der Marel R. P., 1991, MNRAS, 253, 710
van Dokkum P. G., Stanford S. A., 2003, ApJ, 585, 78
van Zee L., Barton E. J., Skillman E. D., 2004, AJ, 128, 2797
Vazdekis A., 1999, ApJ, 513, 224
Vazdekis A., Casuso E., Peletier R. F., Beckman J. E., 1996, ApJS, 106, 307
Vazdekis A., Peletier R. F., Beckman J. E., Casuso E., 1997, ApJS, 111, 203
Worthey G., 1994, ApJS, 95, 107
Zhang F. H., Han Z. W., Li L. F., Hurley J. R., 2005a, MNRAS, 357, 1088
Zhang F. H., Li L. F., Han Z. W., 2005b, MNRAS, 364, 503
Zhou X., Véron-Cetty M.-P., Véron P., 1992, Acta Astrophys. Sin., 12, 308